

**Effective topical treatments of innovative NNO-tridentate vanadium (IV) complexes-mediated photodynamic therapy in psoriasis-like mice model**

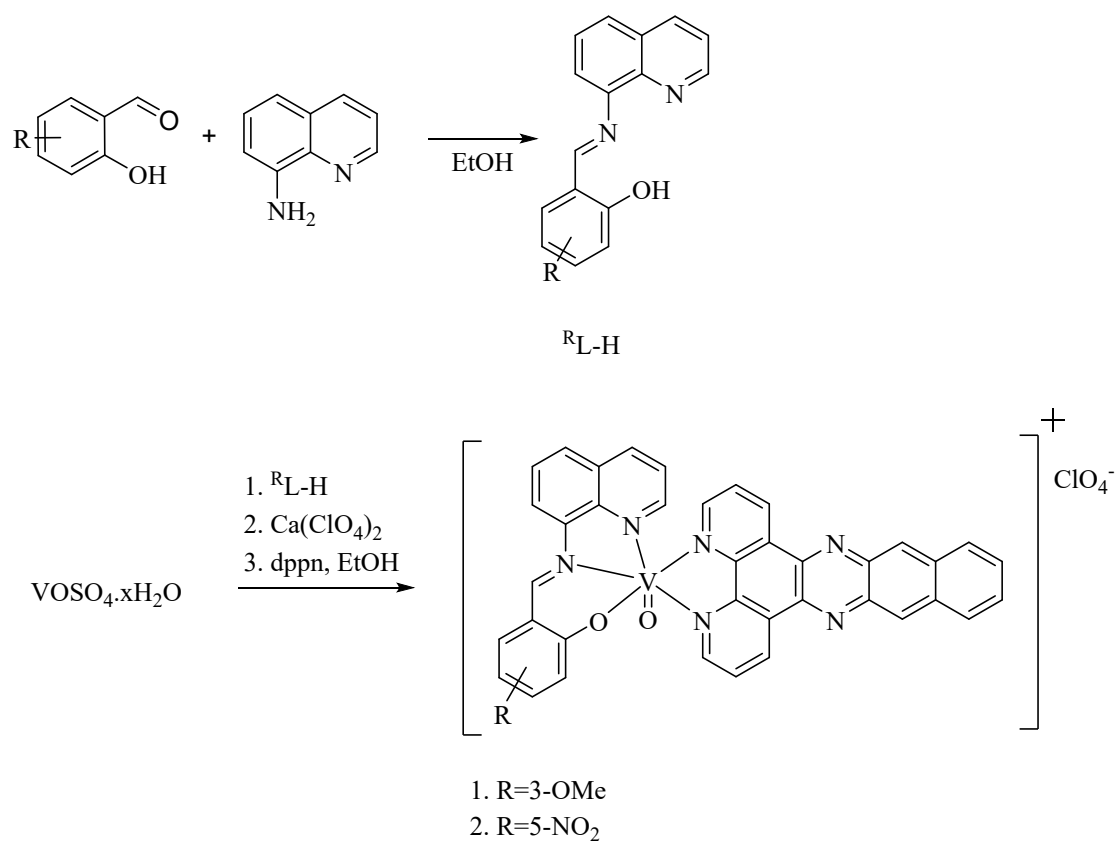
*Rong-Kai Lin,<sup>a</sup> ‡ Parthiban Venkatesan,<sup>a</sup> ‡ Chao-Hsuan Yeh,<sup>a</sup> Ching-Ming Chien,<sup>a</sup> Te-Shan Lin,<sup>a</sup> Chi-Chen Lin,<sup>b</sup> Chu-Chieh Lin,<sup>a\*</sup> and Ping-Shan Lai,<sup>a,c\*</sup>*

**a** Department of Chemistry, National Chung Hsing University, No. 145, Xingda Road, Taichung 402, Taiwan

**b** Institute of Biomedical Science, National Chung-Hsing University, No. 145, Xingda Road, Taichung 402, Taiwan

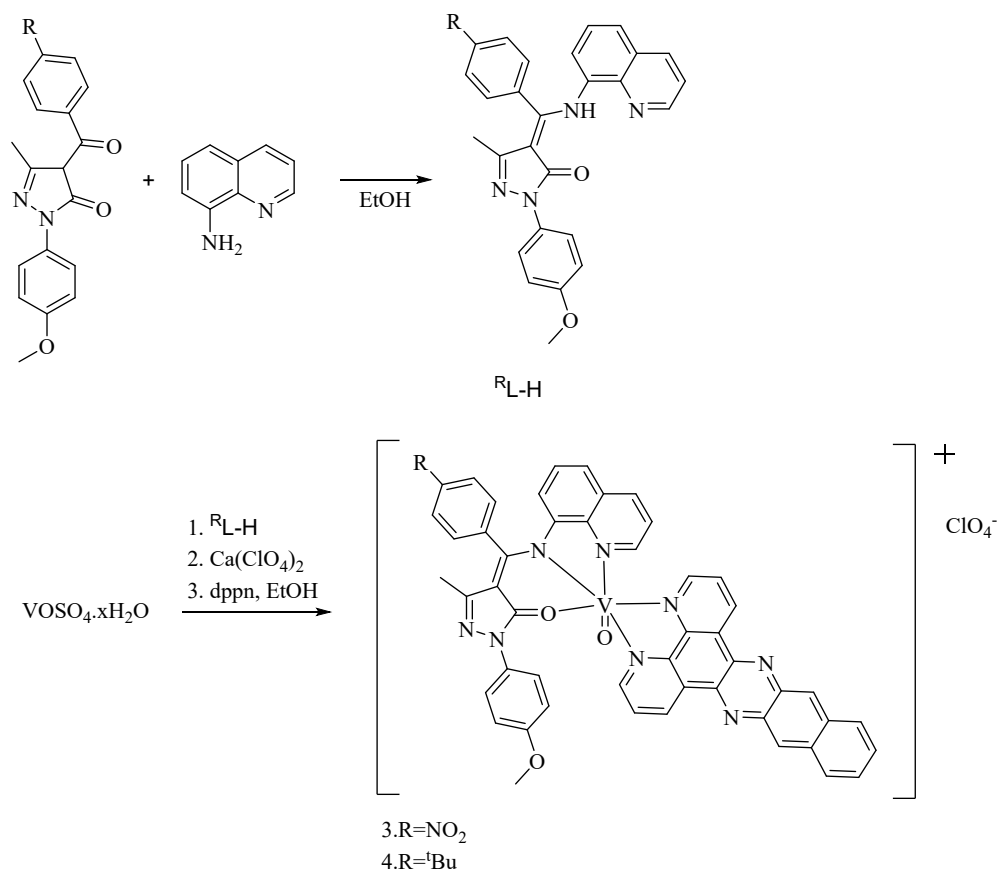
**c** Ph.D. Program in Tissue Engineering and Regenerative Medicine, National Chung Hsing University, No. 145, Xingda Road, Taichung 402, Taiwan.

‡ These authors contributed equally to this work.



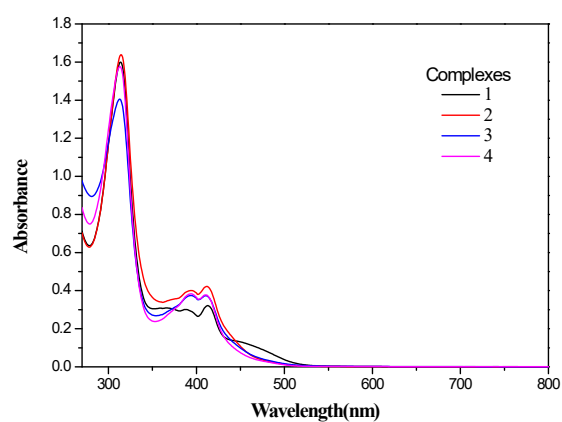
**Schem**

**e S1.** Synthetic routes of ligands  $R_L-H$  and their vanadium complexes **1** and **2**.

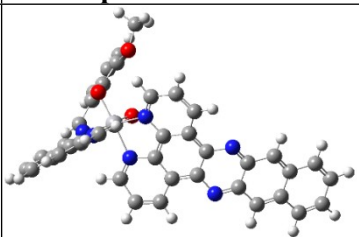
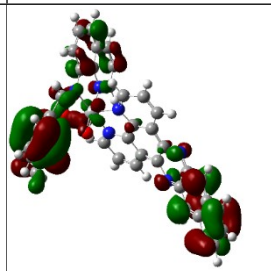
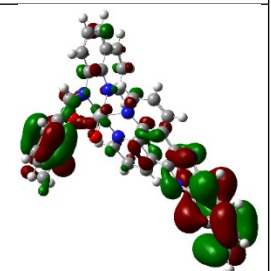
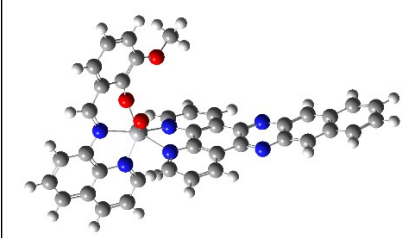
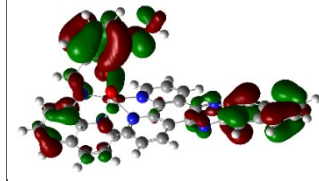
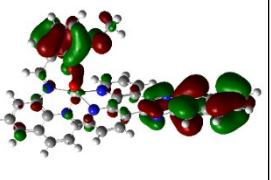
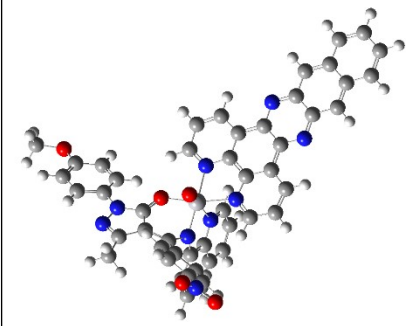
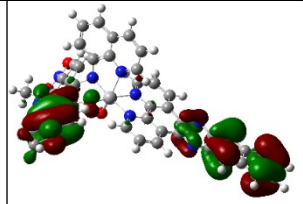
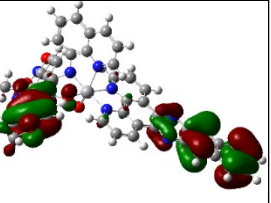


**Schem**

**e S2.** Synthetic routes of ligands  $R_L-H$  and their vanadium complexes **3** and **4**.



**Figure S1.** UV/Vis absorption spectra of complexes (1-4)

Complexes	Optimized structures	HOMO	LUMO
Complex-1		 -15.6669 $\Delta E=0.22\text{eV}$	 -15.4443
Complex-2		 -15.3513 $\Delta E=0.57\text{eV}$	 -14.7741
Complex-3		 -14.6805 $\Delta E=0.22\text{eV}$	 -14.4595

**Figure S2.** Optimized structures of HOMO and LUMO of the complexes 1-3

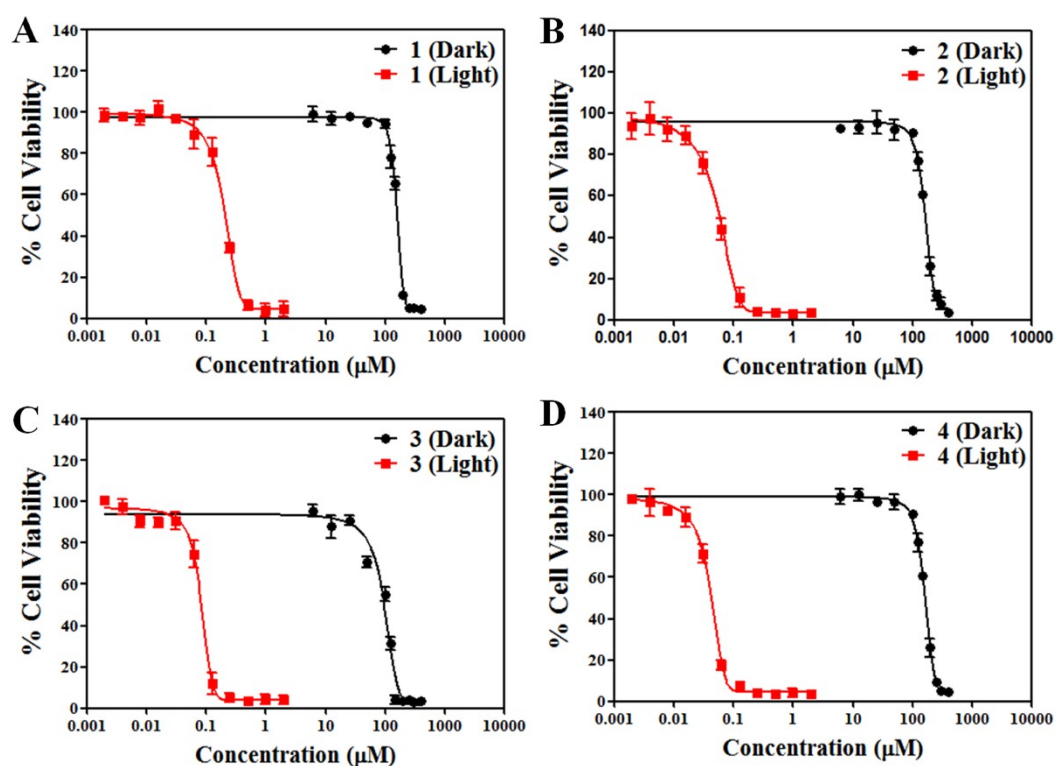


**Figure S3.** Cell viability plots showing the cytotoxicity of vanadium complexes 1-4 against BCC cells in the dark (black symbols) and under blue light (430 nm, 10 min): A to D indicates cytotoxicity of complexes 1-4, respectively.

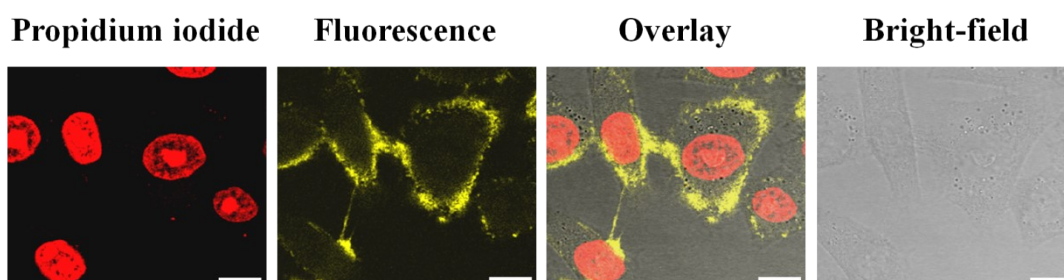
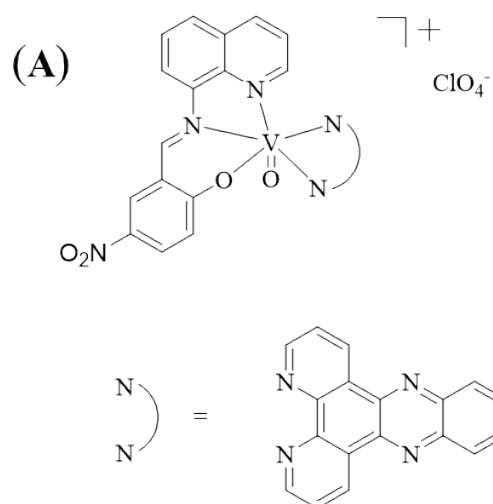


**Figure S4.** Cell uptake of complex **4** in BCC cells. Fluorescence images of complex **4** under confocal microscope after 30 minutes of incubation. Nuclei were stained with Propidium iodide (red). Scale bar 10  $\mu\text{m}$ .



(B)

Lane	1	2	3	4	5	6	7	8	9
Form II									
Form III									
Form I									
	ctrl	dark	air	$\text{NaN}_3$	$\text{D}_2\text{O}$	TEMP	DMSO	KI	SOD
Form II	6.1	10.8	30.1	31.9	53.6	35.3	81.8	31.8	45.9
Form III							14.2		
Form I	93.9	89.2	69.9	68.1	46.4	64.7	4.0	68.2	54.1

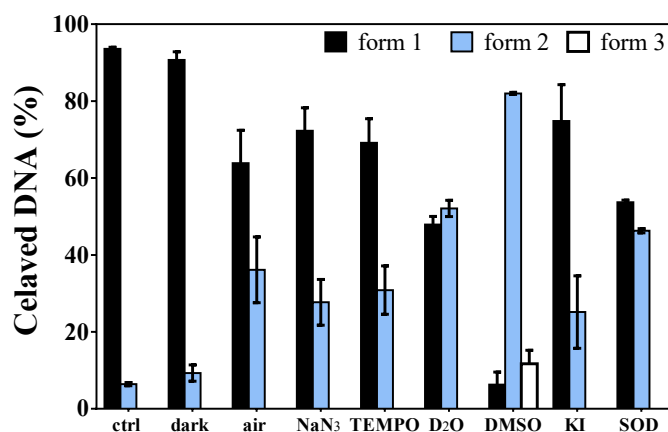


**Figure S5. (A)** Structure of control complex (R- NO<sub>2</sub>) N, N, O-pyrazolonate ligand (in dppz) **(B)** Gel electrophoresis showing the DNA cleavage activity of control complex (50  $\mu$ M) in the blue light of 365nm using SC pUC19 DNA (0.2  $\mu$ g, 30  $\mu$ M b.p.) for an exposure time of 30 min. Addition of different additives NaN<sub>3</sub>(200  $\mu$ M), D<sub>2</sub>O(7 $\mu$ L), DMSO(4 $\mu$ L), KI(200  $\mu$ M), SOD(4 units)

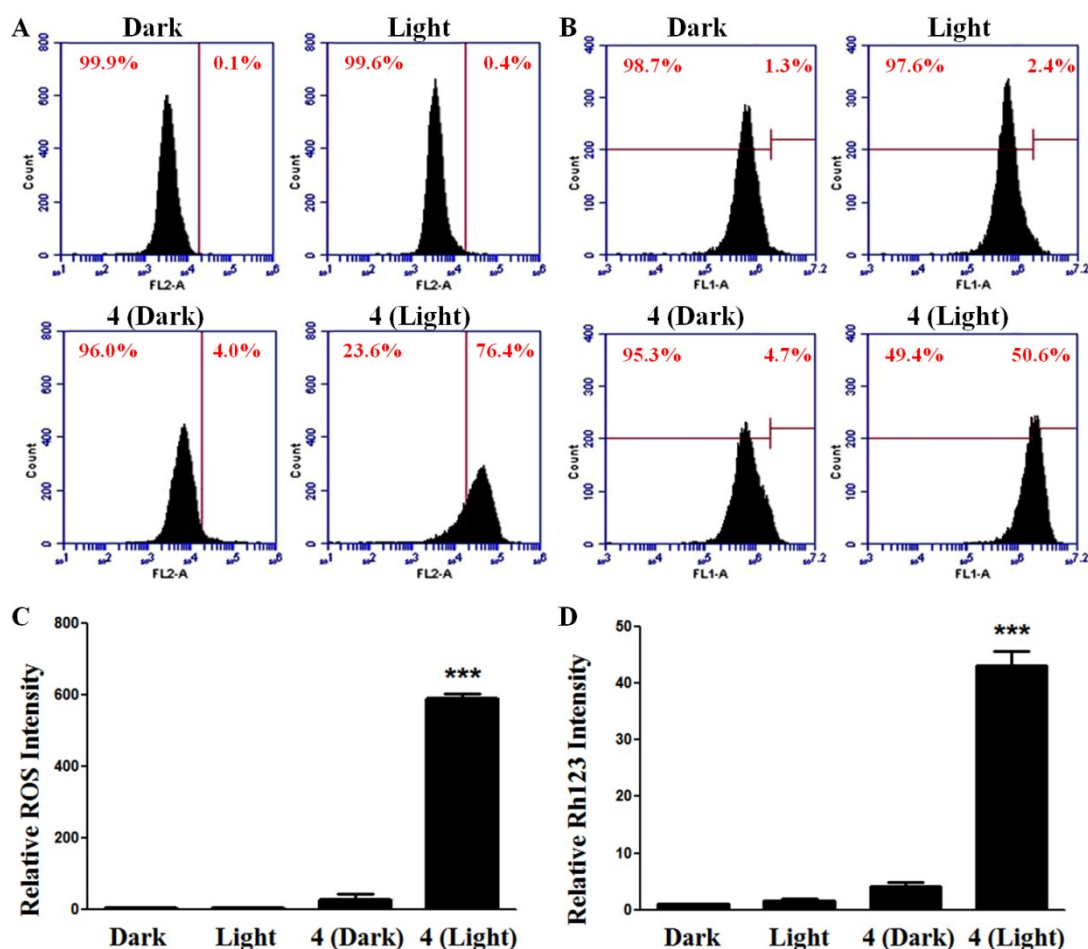


**Figure S6.** Flow cytometry analysis of BCC cells treated with complex 4. (A) and (B) shows flow cytometry analysis of Reactive Oxygen Species (ROS) and Mitochondrial

Membrane Potential (MMP) generation, respectively. Bar diagram (C and D) shows the ROS and MMP activation (as an n-fold increase) compared to that in the dark, respectively. Values are the mean  $\pm$  SD (n = 3). The asterisks represent significantly different values from the control (P<0.001).

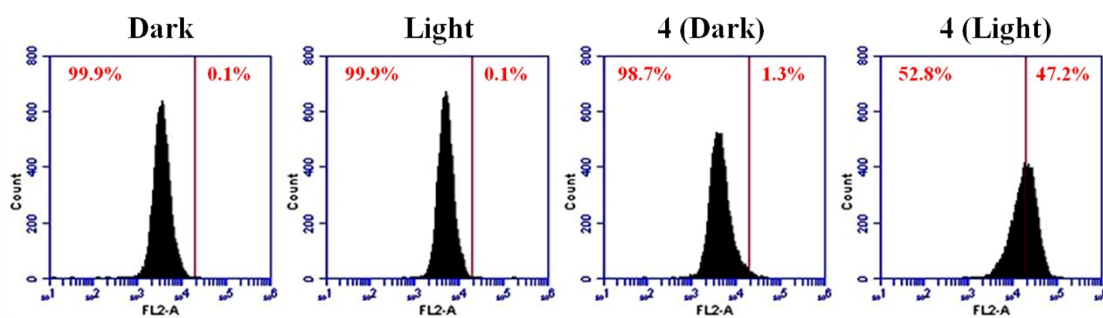


**Figure S7.** Flow cytometric analysis of caspase-3 activation. BCC cells treated with complex 4 as mentioned in materials and methods

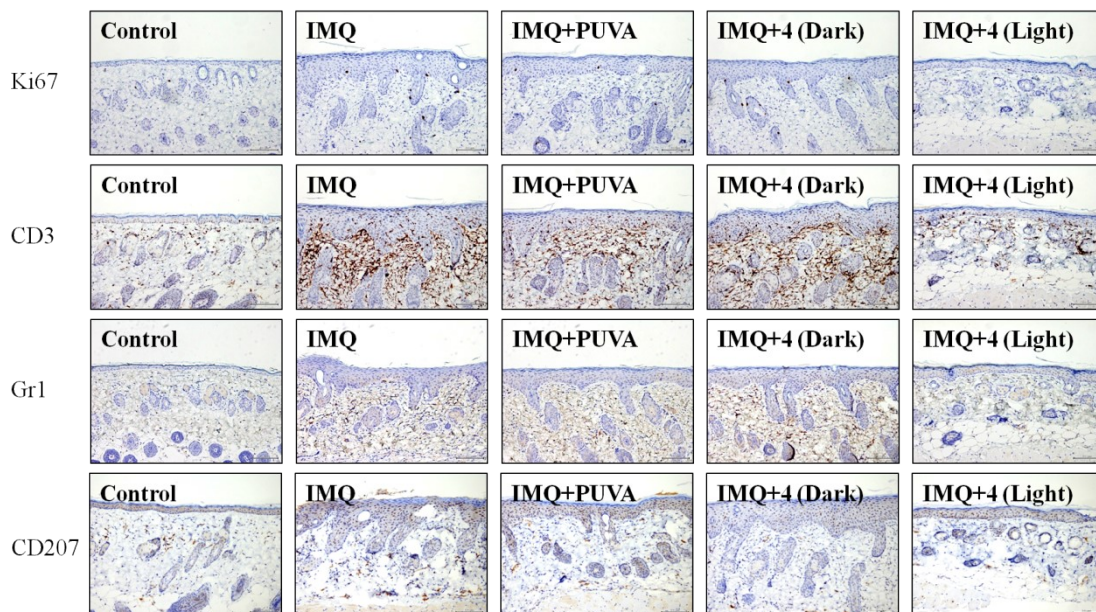


**Figure S8.** Back lesion skin was analyzed by immunohistochemistry. Composition of the epidermal hyperproliferation and leukocyte infiltrate were analyzed using the markers Ki67, CD3 (T cells), Gr1 (neutrophils), and CD207 (Langerhans cells). Scale bar 100  $\mu$ m.

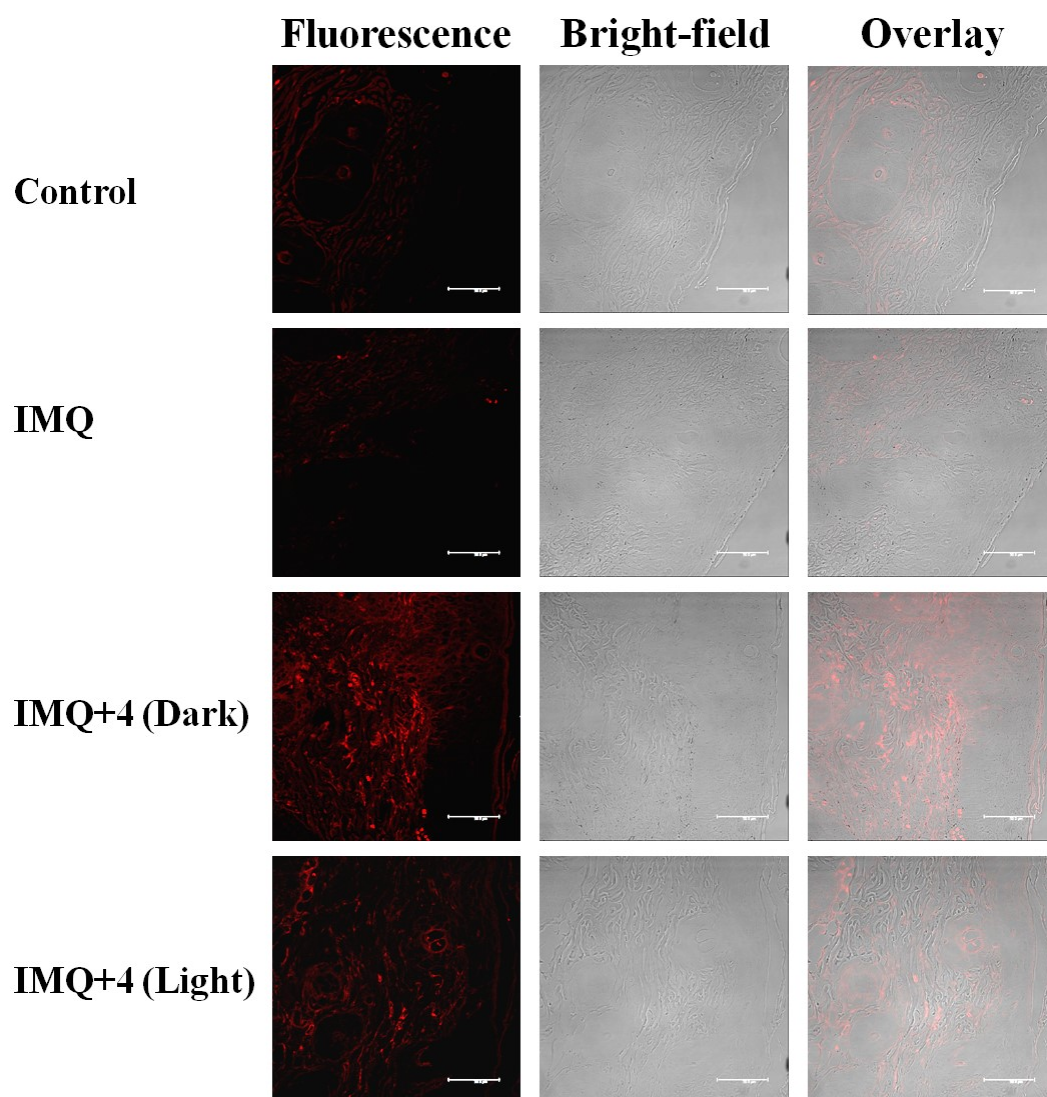


**Figure S9.** The transdermal drug delivery system has shown complex **4** in the mouse skin section. Fluorescence images of complex **4** under a confocal microscope (red). Scale bar 50  $\mu\text{m}$ .

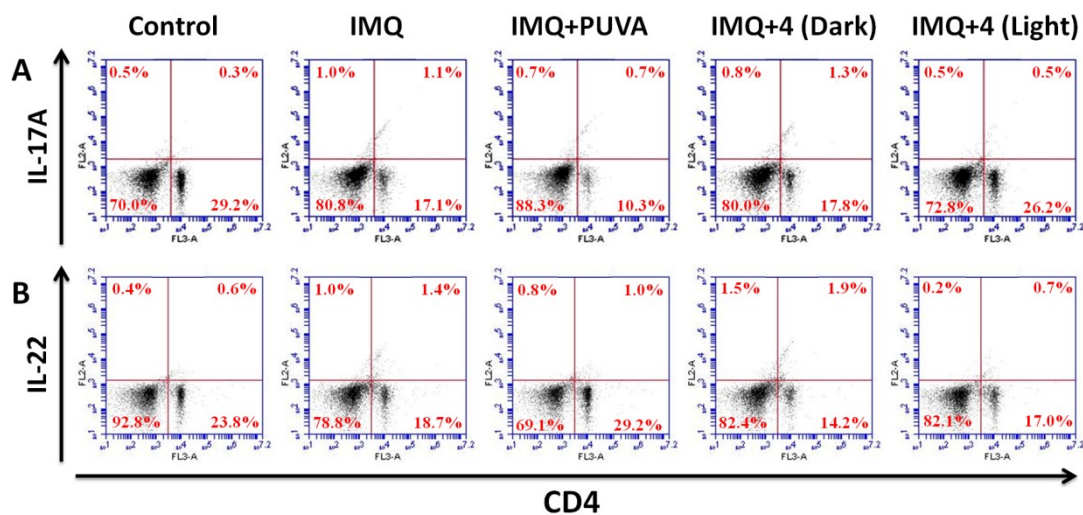


**Figure S10.** Flow cytometric analysis of intracellular IL-17A and IL-22 expression in the spleen. Cells were gated for CD4. The dot plot shows data from one representative mouse of each group. (A) IL-17A-producing CD4<sup>+</sup> T cells. (B) IL-22-producing CD4<sup>+</sup> T cells.

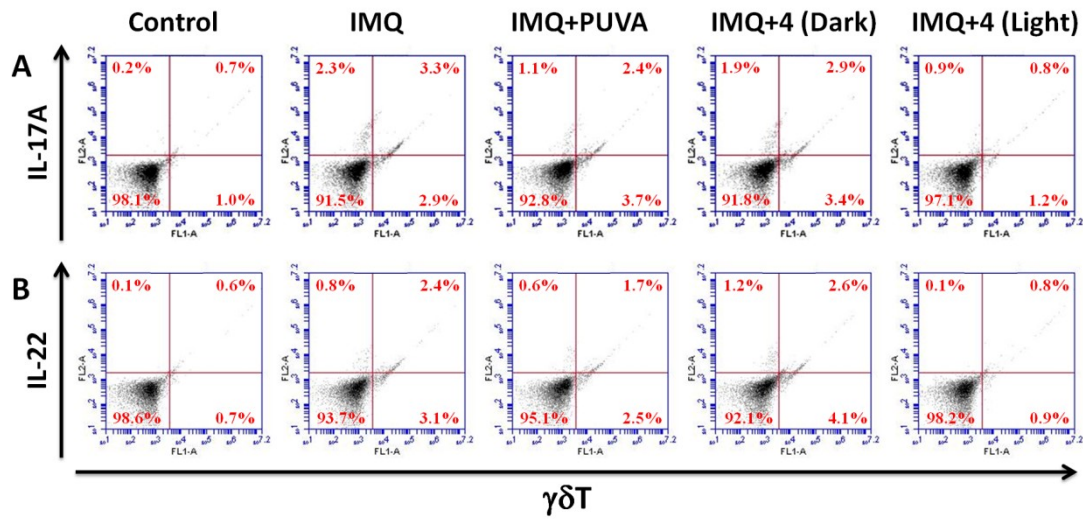
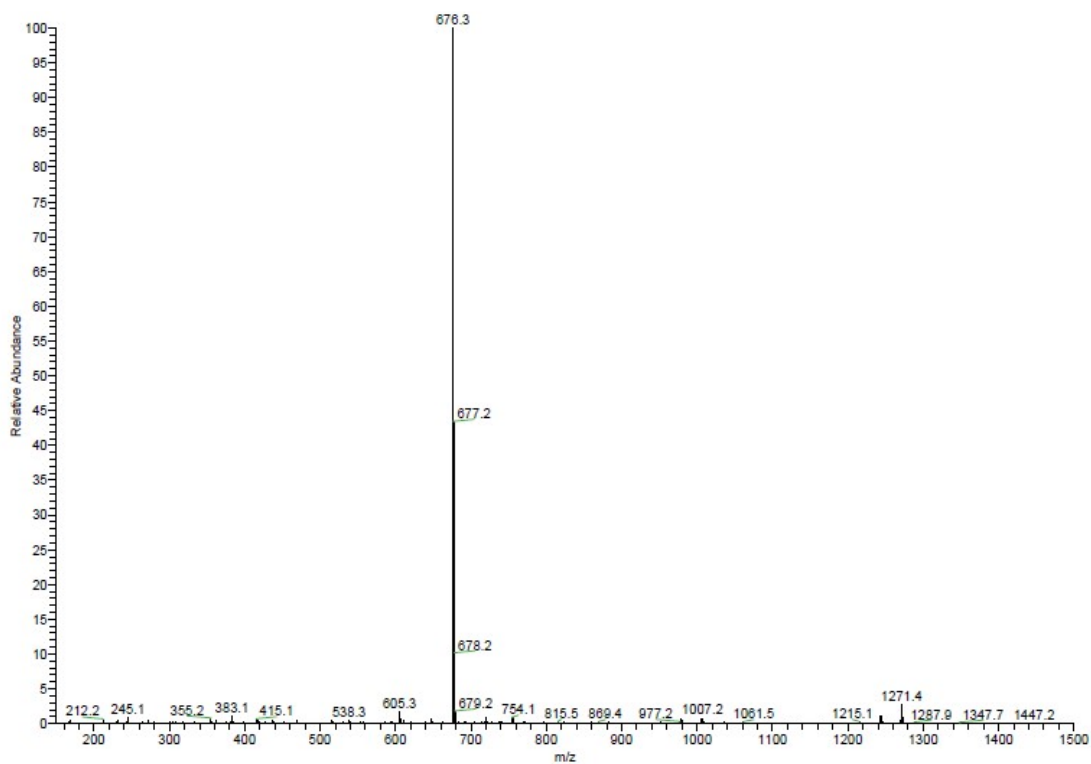


**Figure S11.** Flow cytometric analysis of intracellular IL-17A and IL-22 expression in the spleen. Cells were gated for  $\gamma\delta$ T. The dot plot shows data from one representative mouse of each group. (A) IL-17A-producing  $\gamma\delta$ T cells. (B) IL-22-producing  $\gamma\delta$ T cells.

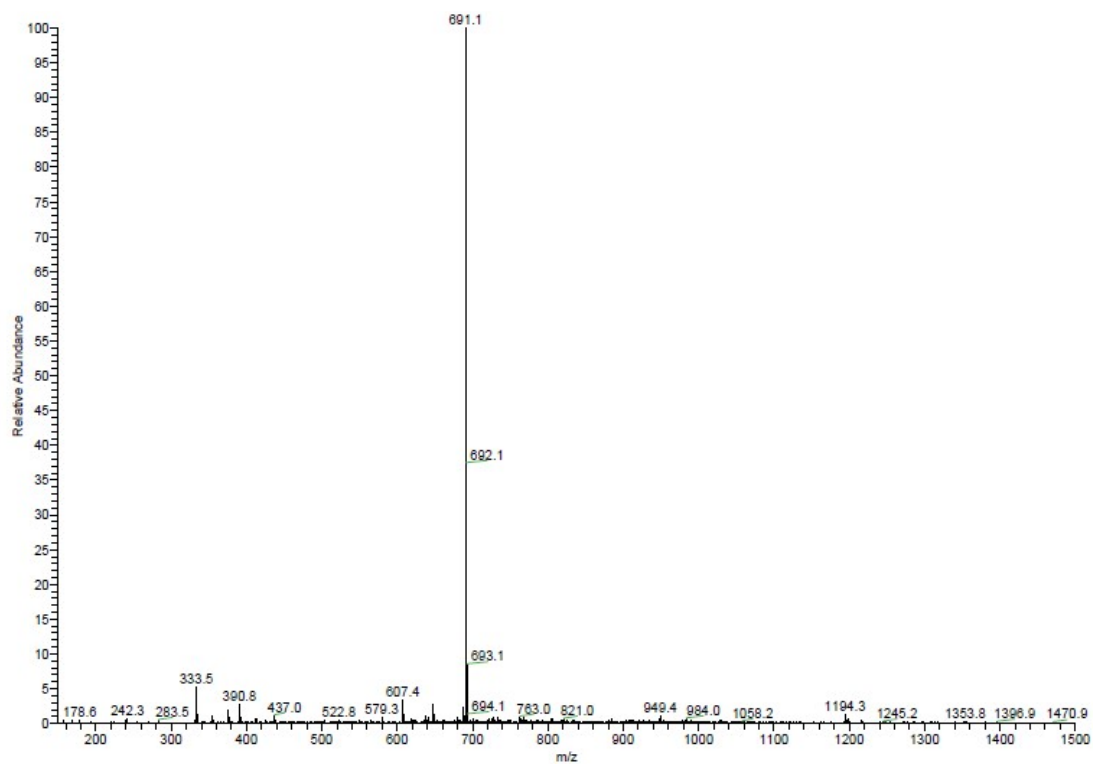
**Table. S1** Comparative thickness of the epidermis and number of cell layers from the back of IMQ-induce psoriasis mice treated with complex **4**.

<b>Mice group</b>	<b>Epidermal thickness (mm)</b>	<b>Number of epidermal cell layers</b>
Control	30.9 ± 2.1	2.4 ± 0.5
IMQ	90.0 ± 11.7	10.3 ± 1.1
IMQ+PUVA	71.0 ± 13.7	8.1 ± 0.9
IMQ+ <b>4</b> (Dark)	83.8 ± 13.4	9.7 ± 0.8
IMQ+ <b>4</b> (Light)	47.1 ± 6.0	4.7 ± 0.5

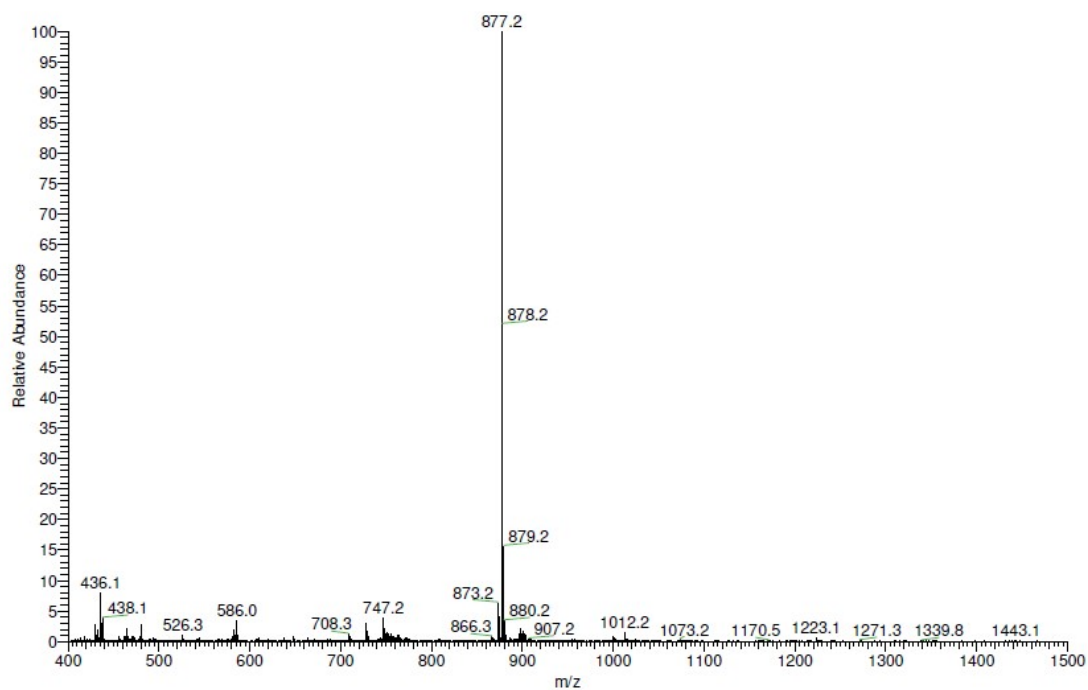
## ESI information



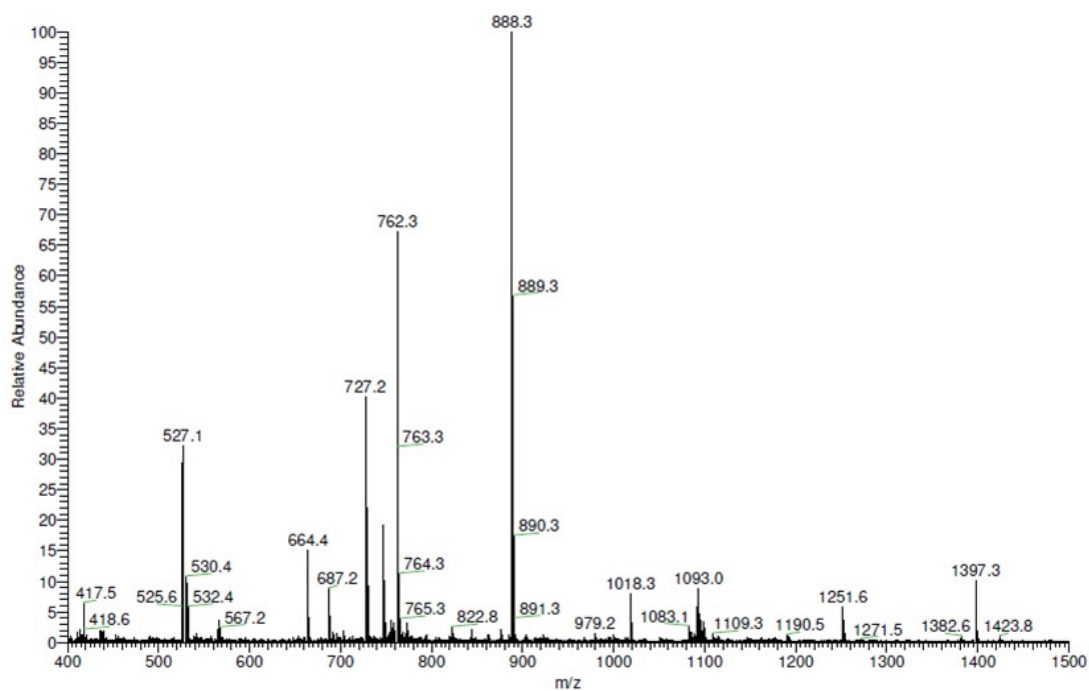
**ESI-Figure 1.** The ESI-MS spectrum of  $[\text{VO}(\text{}^3\text{-OMeL})\text{dppn}]$  (**1**) in DMSO shows a prominent peak corresponding to  $[\text{M-ClO}_4]^+$  at 676 (m/z).



**ESI-Figure 2.** The ESI-MS spectrum of  $[\text{VO}(\text{}^5\text{-NO}_2\text{L})\text{dppn}]$  (**2**) in DMSO shows a prominent peak corresponding to  $[\text{M-ClO}_4]^+$  at 691 (m/z).



**ESI-Figure 3.** The ESI-MS spectrum of  $[\text{VO}(\text{NO}_2\text{L})\text{dppn}]$  (**3**) in DMSO shows a prominent peak corresponding to  $[\text{M}-\text{ClO}_4]^+$  at 877 (m/z).



**ESI-Figure 4.** The ESI-MS spectrum of  $[\text{VO}(\text{tert-butylL})\text{dppn}]$  (**4**) in DMSO shows a prominent peak corresponding to  $[\text{M}-\text{ClO}_4]^+$  at 888 (m/z).